ChemPhysChem

Research Article
doi.org/10.1002/cphc.202400327

Chemistry Europe
European Chemical Societies Publishing

www.chemphyschem.org

Reaction Mechanism Catalyzed by the Dissimilatory Sulfite Reductase – The Role of the Siroheme-[4FeS4] Cofactor

Anna Wójcik-Augustyn,*[a] A. Johannes Johansson,[b] and Tomasz Borowski[c]

The present work is another part of our investigation on the pathway of dissimilatory sulfate reduction and covers a theoretical study on the reaction catalyzed by dissimilatory sulfite reductase (dSIR). dSIR is the terminal enzyme involved in this metabolic pathway, which uses the siroheme-[4Fe4S] cofactor for six-electron reduction of sulfite to sulfide. In this study we use a large cluster model containing siroheme-[4Fe4S] cofactor and protein residues involved in the direct interactions with the substrate, to get insight into the most feasible reaction mechanism and to understand the role of each considered active site component. In combination with earlier studies reported in the literature, our results lead to several interesting insights. One of the most important conclusions is that the reaction mechanism consists of three steps of two-electron reduction of sulfur and the probable role of the siroheme-[4Fe4S] cofactor is to ensure the delivery of packages of two electrons to the reactant.

Introduction

Dissimilatory sulfate reduction is one of the oldest cellular metabolic pathways on Earth, occurring for about three billion years.[1,2] This process, in which sulfate constitutes a terminal electron acceptor, is conducted by sulfate reducing bacteria (SRB) found in anaerobic, sulfate-rich environments, such as soil, deep ground water, deep oceans or innards of higher organisms.[1,3–10] The mechanisms governing sulfate reduction appear to be important in context of the biogeochemical sulfur turnover including biodegradation of aromatic pollutants and disposal of heavy atoms from ground water.[1,6,11–13] The dissimilatory reduction of sulfate to sulfide is catalyzed by three cytoplasmic enzymes: ATP sulfurylase (EC 2.7.7.4) activating sulfate to adenosine 5′-phosphosulfate (APS);[1,14–16] adenosine 5′-phosphosulfate reductase (APSR, EC 1.8.99.2), which cleaves APS and reduces it to sulfite and AMP[1,17,18] and dissimilatory sulfite reductase (dSIR, EC 1.8.7.1) carrying out further six electron reduction of sulfite to anionic sulfide.[1,19] Dissimilatory sulfite reductase (dSIR) utilizes six electrons and six protons to reduce sulfite to hydrogen sulfide (Figure 1). It is assumed that electrons required for the dSIR cycle derive from electron transfer chain including cytochromes, periplasmic hydrogenases and membrane-bound redox enzymes.[1,15] The structure of the core of dSIR is described as $(\alpha\beta)_2$ heterotetramer.[1,17] In some dSIR, the $\alpha(50kDa)\beta(45kDa)$ heterodimer is associated with one or two small subunits: $\gamma(11kDa)$, which is proposed to be directly involved in the reduction of sulfite and $\delta(8kDa)$ suspected of having a regulatory role.[18,20–24] In the crystal structure derived from *Desulfovibrio vulgaris* (PDB code: 2v4j)[22] C-terminus of the γ subunit interacts with siroheme-[4Fe4S] cofactor by its conserved cysteine residue (Figure 2), which is proposed to deliver two electrons to an intermediate of sulfite reduction at the active siroheme-[4Fe4S] cofactor.[22,25]

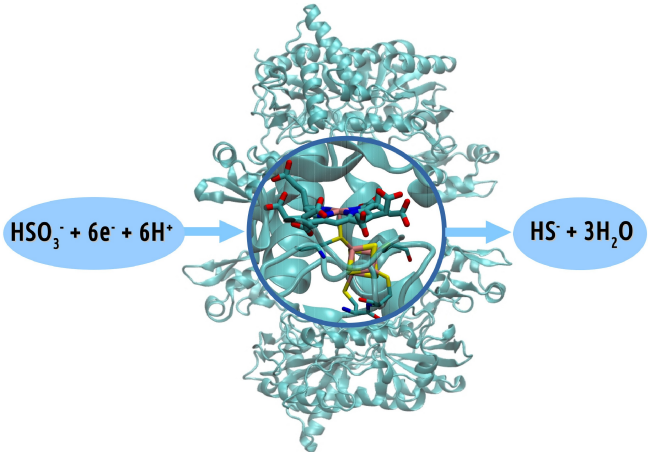

Figure 1. General scheme of sulfite to sulfide reduction catalyzed by dSIR.

The reduction of sulfite to sulfide processed by dSIR enzymes should compensate the cost of sulfate activation catalyzed by ATP sulfurylase (ATPS), thus it must provide ATP molecules to ensure growth.[1] The standard Gibbs free energy change for sulfite to sulfide reduction equals −41.3 kcal/mol, which allows to cover the cost of formation of two moles of ATP.[15] Two different mechanisms have been proposed for the reaction catalyzed by dSIR.[1,19] The first mechanism is direct

[a] *A. Wójcik-Augustyn*
Department of Molecular Biophysics, Faculty of Biochemistry, Biophysics and Biotechnology, Jagiellonian University, ul. Gronostajowa 7, 30-387 Cracow, Poland
E-mail: anna.m.wojcik@uj.edu.pl

[b] *A. J. Johansson*
Swedish Nuclear Fuel and Waste Management Co (SKB), Box 3091, 169 03 Solna, Sweden

[c] *T. Borowski*
Jerzy Haber Institute of Catalysis and Surface Chemistry, Polish Academy of Sciences, ul. Niezapominajek 8, 30-239, Cracow, Poland

Supporting information for this article is available on the WWW under https://doi.org/10.1002/cphc.202400327

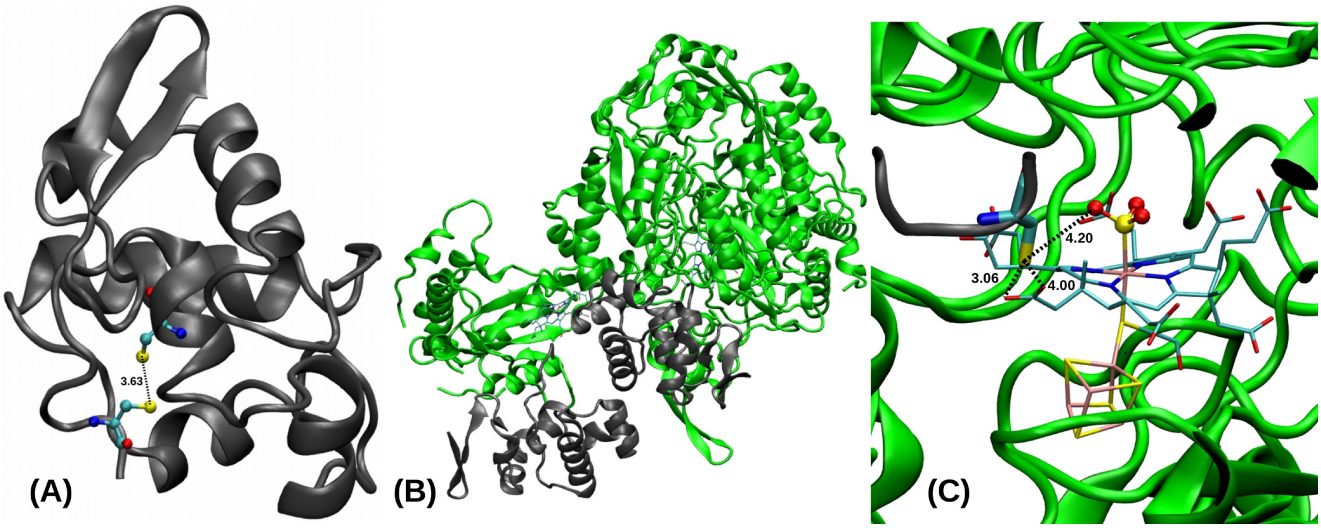

Figure 2. (A) DsrC protein derived from *Archaeoglobus fulgidus* (PDB code: 1sau) with two conserved cysteines hypothesized to provide protons and electrons to dSIR active site; (B) Two DsrC proteins (in grey) bound to $\alpha\beta$ dimer of dSIR (in green) derived from *Desulfovibrio vulgaris* (PDB code: 2v4j); (C) The active site of dSIR from *Desulfovibrio vulgaris* (PDB code: 2v4j) with bound sulfite anion and conserved cysteine residue (thickened licorice) from the C-terminus of DsrC protein (grey cartoon).

reduction of sulfite to sulfide without releasing partially reduced side products, while the second mechanism is called "the trithionate pathway" and allows dissociation of $S_3O_6^{2-}$ and $S_2O_3^{2-}$ intermediates. The mechanistic studies performed for dSIR from *A. fulgidus* in solution and in crystallo revealed that besides sulfide dSIR could produce $S_3O_6^{2-}$ and $S_2O_3^{2-}$, which also might be reduced by the enzyme.[1,25,26] Based on the results three-step mechanism was proposed proceeds through three stages of two-electron and two-proton transfer coupled with the dehydration reactions (Figure 3).[1,25] The formation of trithionate and thiosulfate as side products depends on the stability of intermediates of sulfite reduction, whether they lifetime is long enough to react with another sulfite molecule.[1,25] The activity of dSIR from *D. desulfuricans* was measured for three substrates, i.e. sulfite, trithionate and thiosulfate, at temperature of 83 °C and for pH from 5–8 range.[25] All three substrates revealed maximal activity at pH of 6.0. The activity value determined for sulfite at pH 7.0 agrees with the values reported for dSIR from *A. fulgidus*.[27] Activity obtained for thiosulfate ($S_2O_3^{2-}$) was slightly higher than for sulfite, while trithionate ($S_3O_6^{2-}$) reveals lower activity than sulfite under applied conditions.[25] Product analysis revealed that reduction of sulfite leads to production of trithionate, thiosulfate and sulfide, trithionate reduction provides thiosulfite and sulfide, while thiosulfate reduction produces sulfide. Trials to obtain crystal structures of dSIR in complex with trithionate and thiosulfate failed, most likely because of their fast conversion to sulfide or sulfite.[25] The mixture of sulfide, trithionate and thiosulfate as products of dSIR catalysis was detected after removal of membrane fraction,[22,28] in the whole cell extracts (from *D. vulgaris*) only sulfide product was observed.[22] Additionally, dSIR purified from the membranes produces mainly sulfide, while dSIR extracted from the soluble fraction catalyzes formation of a mixture of three products.[29] From the analysis of the *in vivo* and *in vitro* products and

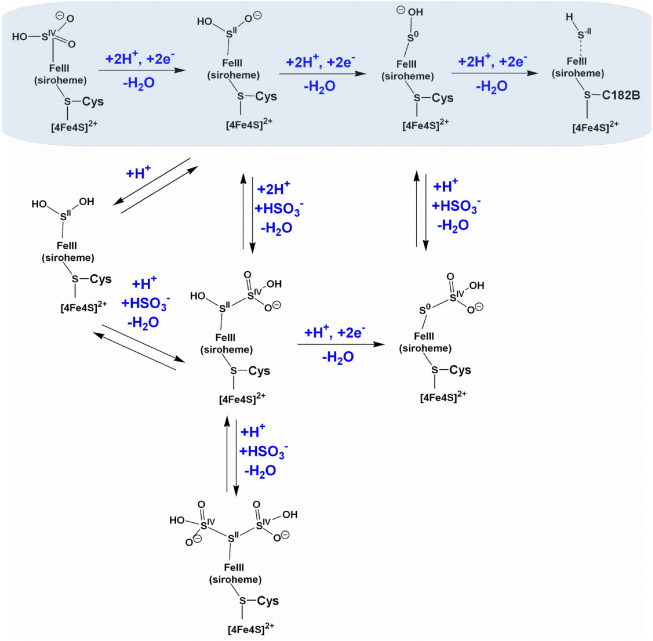

Figure 3. Catalytic reaction catalyzed by dSIR consisting of three steps of coupled two electrons and two protons transfer (light blue background). The scheme includes production of trithionate and thiosulfate as side products formed as a result of electron deficiency (white background).

available crystallographic data[22] (Figure 2), it can be concluded that in dSIR reaction γ subunit, also called DsrC protein, might play an important role. DsrC protein (γ subunit) with highly conserved C-terminus containing two cysteine residues is also considered as separate protein which delivers electrons to siroheme-[4Fe4S] cofactor. DsrC protein might be reduced by the DsrMKJOP membrane complex (disulfide/thiol reductase activity).[22]

Within the $(\alpha\beta)_2$ core of dSIR, α and β subunits reveal similar tertiary structures, which are divided into three domains A1/B1, A2/B2 and A3/B3.[22] A1 and B1 domains consists of four- or five-stranded antiparallel β-sheet, flanked by two α-helices. A1 domain contains additionally two helices at N-terminus. The A2 and B2 domains are arranged in five-stranded β-sheet and several α-helices. The A2 and B2 domains bind [4Fe4S] cluster from siroheme-[4Fe4S] cofactor. In the A2 domain [4Fe4S] is bound in proximity to the catalytically inactive (deprived of iron or blocked by tryptophan residue, see Figure 4) siroheme and coordinated by four cysteines from the $CX_5CX_nCX_3C$ motif, which is strictly conserved in known representatives of sulfite reductases.[27,30] Such "structural" siroheme-[4Fe4S] cofactor is buried in the protein on the interface between α and β subunits. The B2 domain binds another [4Fe4S] cluster, which constitutes "functional" siroheme-[4Fe4S] cofactor, by four cysteines from a different CX_nCCX_3C motif conserved in most dSIR enzymes (exception is dSIR from *P. aerophilum*, which contains $CX_5CX_nCX_3C$ motif in both α and β subunits).[22]

The iron cation within the "functional" siroheme from β subunit is bound to [4Fe4S] cluster by thiolate group of conserved cysteine. This exchange-coupled siroheme-[4Fe4S] cofactor was found at the active sites of enzymes capable of sulfite or nitrite reduction.[31–33] The A3 and B3 domains display ferredoxin fold and are inserted within the A2 and B2 domains from α and β subunits, respectively.[22] They are arranged into two two-stranded β-sheets flanked by three α-helices and bind another [4Fe4S] cluster. In the β subunit this additional [4Fe4S] cluster is coordinated by four cysteine residues and positioned about 6 Å from protein surface and about 13 Å from catalytically active siroheme-[4Fe4S] cofactor, which indicates its possible role in transfer of electrons from external source to the catalytic site (Figure 5).[22] Comparison of the available crystal structures of dSIR derived from *D. vulgaris*, *D. gigas* and *A. fulgidus* revealed that the overall structure of $(\alpha\beta)_2$ hetero-tetramer from *A. fulgidus* is similar to that of *D. vulgaris* and *D. gigas*, with only small difference in the N- and C-terminal fragment of α and β subunits and two longer loops in the ferredoxin domains (A3/B3).[22] The most important difference is presence of the iron in the "structural" siroheme-[4Fe4S] cofactor in dSIR from *A. fulgidus* in comparison to sirohydrochlorins deprived of iron in the corresponding sites of *D. vulgaris* and *D. gigas* (Figure 4). Both "structural" and "functional" cofactors are located in the interface between α and β subunits. The catalytically active siroheme-[4Fe4S] cofactor is surrounded by strictly conserved residues: Rα80, Kα215, Rα229, Rα358, Rα360 in *A. fulgidus* (Rα83, Kα217, Rα231, Rα376, Rα378 in *D. gigas* and *D. vulgaris*) interacting with carboxyl groups of siroheme and Rα98, Rα170, Kα211, Kα213 in *A. fulgidus* (Rα101, Rα172, Kα213, Kα215 in *D. gigas* and *D. vulgaris*, Figure 4) engaged in strong electrostatic interactions with oxygen atoms of sulfite. These latter four residues are proposed to deliver some of protons required for sulfite reduction.[22] It is hypothesized that during sulfite reduction the active site of dSIR does not undergo major conformational changes.[1] Sulfite ion is bound to the siroheme iron as an axial ligand forming trigonal bipyramidal arrangement and interacts with two arginines and two lysines, which besides delivery of protons can facilitates release of water molecules.[1,22] Based on results of experimental and theoretical studies, it is proposed that sulfite ion is firstly protonated by water molecule or it is protonated prior binding leading to HSO_3^- ion interacting with iron.[1,34] Spectroscopic and crystallographic studies lead to proposal of mechanism presented in Figure 3, for which several key intermediates have been identified so far.[26,31,34–37]

The siroheme Fe(III)-sulfite adduct has been observed spectroscopically and structurally.[25,36] Sequential reaction steps involving protons and electrons delivery were proposed to lead through $SOOH^-/SO_2^-$ to SOH^- ligand, which upon dehydration process is transformed to the final sulfide product (Figure 3). The exact sequence in which protons and electrons are delivered to the active site is debatable, thus DFT calculations were performed by Silaghi-Dumitrescu and Makarov to analyze the path of sulfite reduction catalyzed by dSIR.[34] In this computational study, small model of dSIR active site was used, containing siroheme without any lateral substituents, sulfite/sulfide ion and methyltiolate ligand coordinating heme and iron-sulfur cluster. The [4Fe4S] cluster was not included in the

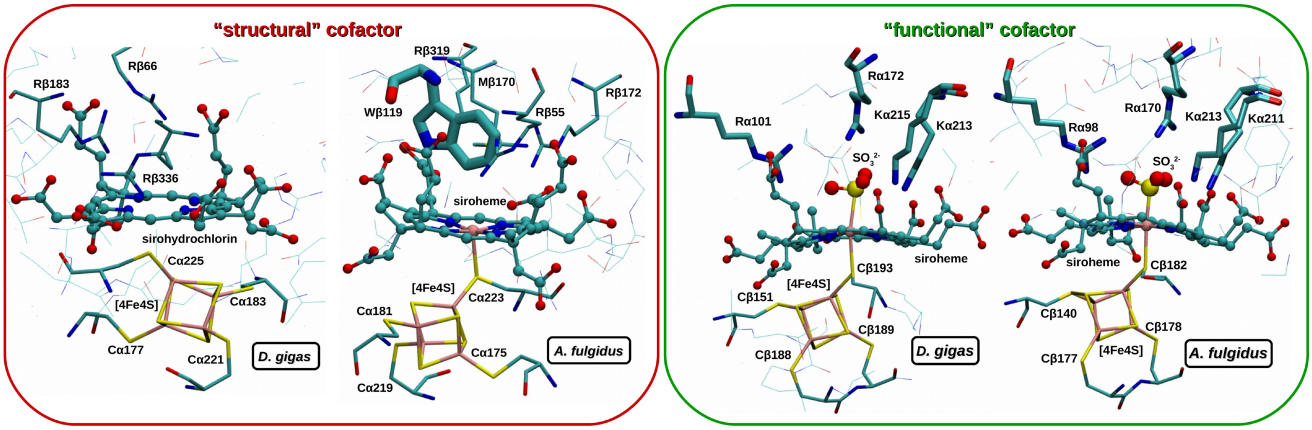

Figure 4. The binding sites of "structural" (red frame) and "functional" (green frame) siroheme-[4Fe4S] cofactor within the crystal structures of dSIR from *Desulfovibrio gigas* and *Archaeoglobus fulgidus*.

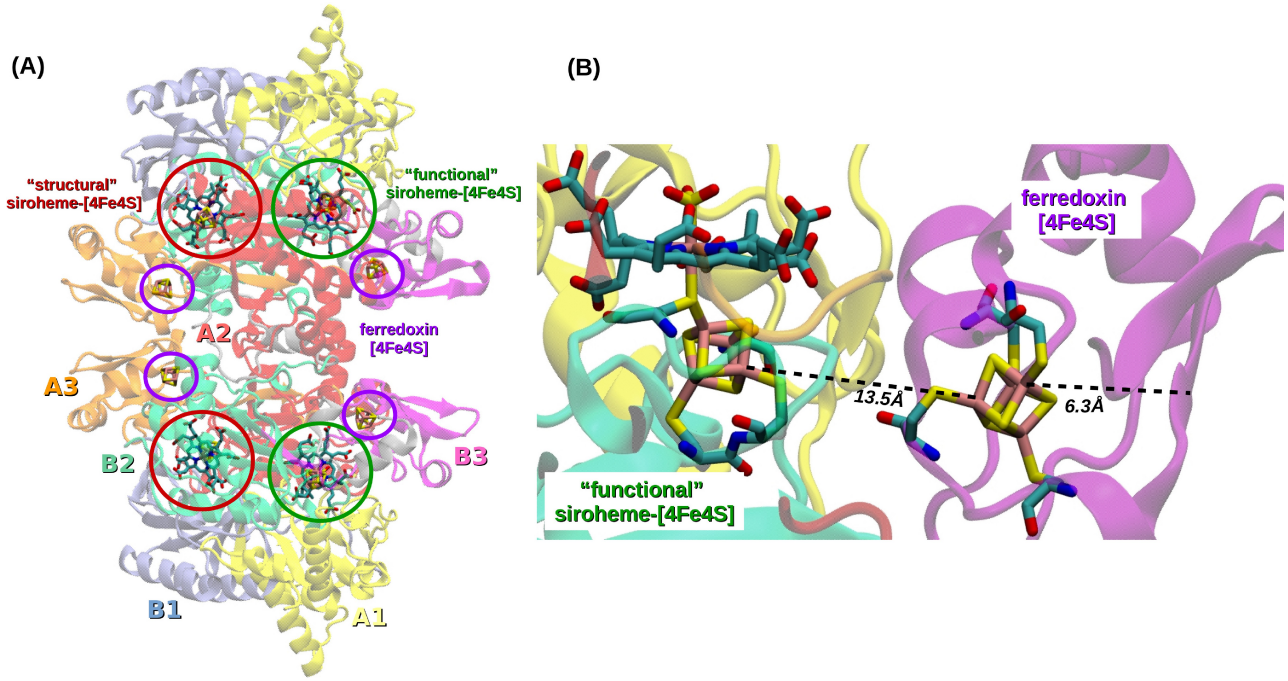

Figure 5. (A) The structure of $(\alpha\beta)_2$ tetramer derived from *Archaeoglobus fulgidus* (PDB code: 3MM5) with marked structural domains: A1 (yellow), A2 (red), A3 (orange), B1 (light blue), B2 (green), B3 (magenta), binding sites of "structural" (red frames) and "functional" (green frames) siroheme-[4Fe4S] cofactors and [4Fe4S] clusters in A3/B3 ferredoxin domains (purple frames); (B) Relative position of the "functional" siroheme-[4Fe4S] cofactor and ferredoxin [4Fe4S] cluster within the structure from Figure (A).

considered QM model according to the assumption that its role is limited to channeling electrons to the siroheme iron. The DFT study revealed several possible pathways. The proposed mechanism starts with Fe(III)-HSO_3^-, which by protonation and dehydration is transformed to Fe(III)-SO_2^0. The subsequent steps include one electron reduction to Fe(III)-SO_2^-, which after delivery of two protons and release of water molecule is transformed to Fe(III)-SO^+. Afterwards, the Fe(III)-SO^+ accepts three electrons and Fe(II)-SO^- is formed, from which after delivery of three protons Fe(IV)-SH is formed.[34]

The spectroscopic EPR experiments indicated that the resting state of sulfite reductases has high-spin ferric (S = 5/2) form of siroheme, which might be reduced to high spin ferrous state (S = 2).[38,39] The electronic structure of the [4Fe4S] cluster was determined by Mössbauer spectra; two Fe ions forming a cubane face are ferromagnetically coupled (S = 9/2) and two such pairs interact antiferromagnetically.[40] Moreover, theoretical study performed for the models of the siroheme-[4Fe4S] cofactor revealed that states with antiferromagnetic coupling between siroheme iron and the closest [4Fe4S] iron are more stable than those where these iron ions are ferromagnetically coupled.[38] The DFT study was performed to evaluate the role of [4Fe4S] cluster in control of spin state of siroheme iron, the effect of replacement of siroheme by heme moiety, and the impact of cysteine bridging siroheme iron and [Fe4S4] cluster.[38] The obtained results showed that siroheme ring stabilizes high- and intermediate-spin state of central iron. Moreover, the siroheme-[4Fe4S] cofactor provides more negative reduction potential in comparison to heme. The interaction between siroheme Fe(II) and bridging cysteine was stronger than corresponding heme Fe(II)-Cys, while the opposite effect was observed for models containing Fe(III) siroheme/heme species. Importantly, the presence of the [4Fe4S] cluster in the model significantly strengthens this bond in the models containing ferric siroheme/heme state. The model containing Fe(II) siroheme/heme iron and [4Fe4S] cluster revealed the weakest iron-Cys interaction. It was found that the most stable states have opposite spins on siroheme iron and the closest iron from iron-sulfur cluster. Summarizing, presence of siroheme instead of heme was found to be crucial for SIR activity. Ligand field interactions between iron and coordinating atoms are decreased in systems containing siroheme, which causes stabilization of the high spin states. In a recent theoretical study it was found that the presence of the [4Fe4S] cluster in the dSIR active site influences the electronic properties of siroheme by increasing its electrophilicity, which in turn strengthens the interaction between the siroheme group and the substrate.[41]

The theoretical study performed so far on the dSIR reaction mechanism[34] applied a small model, which did not include [4Fe4S] cluster and active site residues; the latter most likely play an important role as proton donors and reaction regulators. The results indicated several possible reaction pathways for sulfite reduction and did not provide any information about the source of required protons and electrons.

The QM cluster approach is the main theoretical method used to study reaction mechanisms catalyzed by metalloenzymes. Its application has enriched our knowledge about many redox processes and enabled the interpretation of spectro-

scopic, crystallographic and mutagenic results.[42–44] Nowadays, it is possible to effectively use large models (over 200 atoms), which if designed appropriately, show very good accuracy in reproduction of the results of experimental studies.[45] In the present study, we explored the reaction energy landscape with the use of a more complete active site model, which provided insight into the structure of the most stable dSIR reaction intermediates. We also learned about the role of [4Fe4S] cluster in the catalysis and checked which active site residues might be directly involved in sulfite reduction as proton donors.

Models and Methods

Three cluster models of dSIR active site were constructed based on the crystal structure of *Archaeoglobus fulgidus* dSIR in complex with sulfite ion (PDB code: 3MM5), i.e. small model, medium model and large model (Figure 6, Supplementary Data). The mechanism of dSIR reduction was modeled using the medium model, while the small and large models were applied to understand the properties of the siroheme-[4Fe4S] cofactor and its sensitivity to the protein environment. Small model (99 atoms) contains only siroheme with its propionates replaced by methyl groups, [4Fe4S] cluster and its four cysteine ligands (Cβ140, Cβ177, Cβ178, Cβ182) with their Cα atoms replaced by hydrogens. The medium model (184–190 atoms, Figure 7), which is considered to be sufficiently large to preserve key properties of the active site, contains HSO_3^- anion, three water molecules, siroheme with propionate moieties replaced by methyl groups, [4Fe4S] cofactor, Rα98, Rα170, Kα211, Kα213 from α subunit and Cβ140, Cβ177, Cβ178 and Cβ182 from β subunit with their Cα carbons replaced by hydrogen atoms. The large model (255 atoms) in addition to the components of the medium model also contains seven residues from the [4Fe4S] cluster surroundings, belonging to the β subunit, i.e. Tβ134, Qβ135, Gβ136, Wβ137, Tβ142, Pβ143, Nβ180. For the Tβ134-Wβ137 fragment, the protein backbone and the side chain of Tβ134 were included, whereas side chains of Qβ135 and Wβ137 were replaced with hydrogen atoms. In the case of Tβ134 its amino group and for Wβ137 its carbonyl group from protein backbone were replaced by hydrogen atoms. For Tβ142-Pβ143 dipeptide, the amino group of Tβ142 and the carbonyl group of Pβ143 from protein backbone were replaced with hydrogen atoms, while Nβ180 was included with Cα replaced by hydrogen atom. In the large and medium models, the sulfite anion was protonated on the oxygen facing the water channel (Figure 7). During geometry optimization of all models constraints were imposed on Cβ carbons, hydrogen atoms replacing Cα, Cβ carbons, CO and NH moieties from protein backbone and carboxyl groups in siroheme. The protonation states of the residues included in the models were estimated based on the pKa evaluation performed with the Propka 3.1 program.[46,47] Thus in physiological conditions (pH = 7.0), Rα98 (pKa = 12.97), Rα170 (pKa = 11.33), Kα211 (pKa = 9.67) were fully protonated (positively charged), while Kα213 (pKa = 6.59) was included in its neutral state. Since Kα213 and Kα211 interact with each other, within this study, we tested structures containing either Kα211 or Kα213 deprotonated to present the most stable geometries in this manuscript. Some fully protonated models were also tested in order to model a proton-rich environment.

All quantum mechanical (QM) calculations were performed with Gaussian 16 program.[48] Geometries of considered stationary points were optimized using DFT/B3LYP (hybrid exchange-correlation functional) method combined with D3 Grimme's correction for van der Waals interactions[48,49] computed with the Becke-Johnson damping[50] and def2-SVP basis set.[51] This method was suggested for models containing siroheme-[4Fe4S] complex by Branzanic et al.[38] The final energies of optimized geometries were computed as a combination of DFT-B3LYP-D3/def2-TZVP energies computed with the polarisable continuum model (PCM) of protein environment (the integral equation formalism variant with dielectric constant of 4.0 and radius probe of 1.4[52]) and zero-point energy corrections computed from vibrational analysis performed on the DFT-B3LYP-D3/def2-SVP level of theory.

Results and Discussion

Multi-sequence alignment for subunit α revealed that two arginine (Rα98 and Rα170 in *A. fulgidus*) and two lysine (Kα211 and Kα213 in *A. fulgidus*) residues directly interacting with sulfite anion (Figure 7C,D), as well as the following residues: Rα80, Tα133, Yα210, Kα215, Kα314, Rα358, Rα360 (numbering from *A. fulgidus*) interacting with the "functional" siroheme are

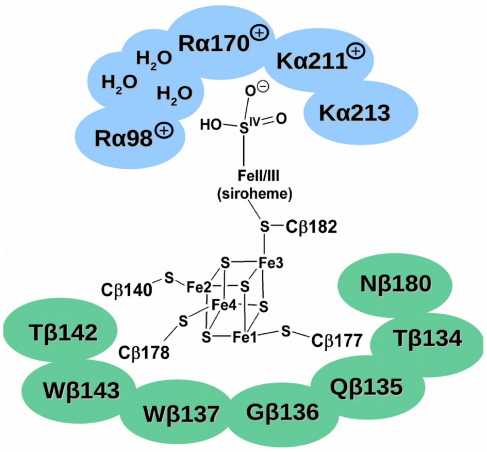

Important spin populations		SMALL		MEDIUM				LARGE	
		ox-empty	red-empty	ox-empty	red-empty	ox-HSO_3^-	red-HSO_3^-	ox-HSO_3^-	red-HSO_3^-
SRM	*Fe(SRM)*	3.77	3.77	3.72	3.72	3.73	3.72	3.75	3.73
	siroheme	0.15	0.12	0.16	0.17	0.15	0.14	0.14	0.13
[4Fe4S]	*Fe1*	3.88	3.70	3.87	3.87	3.88	3.71	3.90	3.68
	Fe2	-3.72	-3.69	-3.76	-3.75	-3.75	-3.77	-3.70	-3.74
	Fe3	-3.67	-3.72	-3.64	-3.65	-3.65	-3.67	-3.69	-3.66
	Fe4	3.87	3.74	3.86	3.86	3.86	3.78	3.89	3.84
	4S	0.42	-0.10	0.20	0.26	0.28	-0.19	0.20	-0.17
ligands of [4Fe4S]	*Cβ140(S)*	-0.23	-0.14	-0.26	-0.25	-0.25	-0.18	-0.19	-0.18
	Cβ177(S)	0.30	0.16	0.39	0.36	0.36	0.14	0.25	0.08
	Cβ178(S)	0.31	0.18	0.39	0.37	0.36	0.23	0.44	0.28
	Cβ182(S)	-0.09	-0.04	0.02	-0.01	-0.01	0.03	0.05	0.00
other	*Rα170*	-	-	0.00	-0.91	0.00	0.00	0.00	0.00

Figure 6. The diagram showing the contents of the small (on white background), medium (on white and blue background) and large (on white, blue and green background) models and the table with important spin populations gathered from optimized geometries of the following versions of dSIR active site: "**ox-empty**" – oxidized siroheme-[4Fe4S] deprived of the sulfite; "**red-empty**" – one-electron reduced siroheme-[4Fe4S] deprived of the sulfite; "**ox-HSO_3^-**" – oxidized siroheme-[4Fe4S] with the sulfite ion bound; "**red-HSO_3^-**" – one-electron reduced siroheme-[4Fe4S] with the sulfite ion bound.

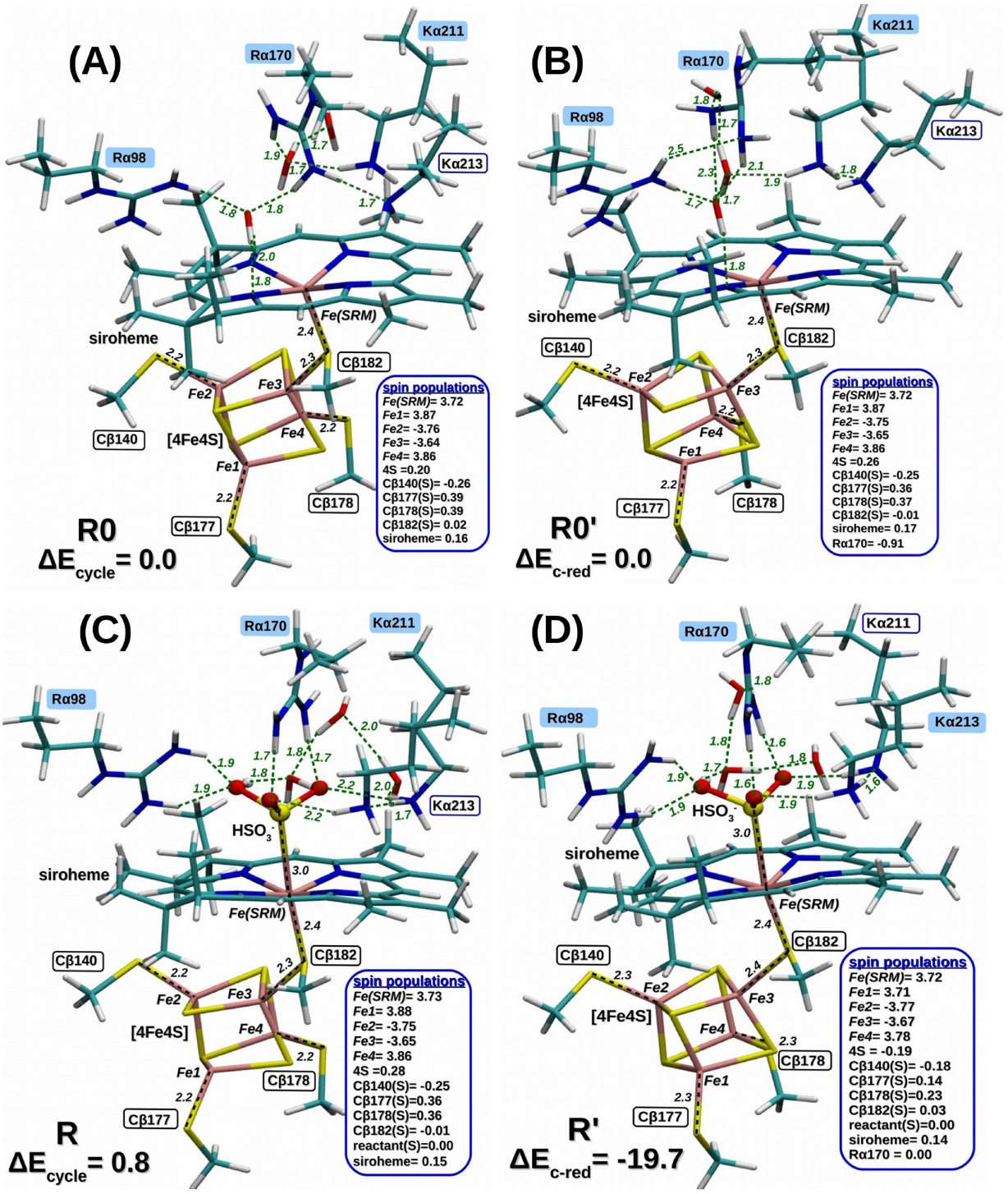

Figure 7. Optimized structures of the medium model: (A) with oxidized siroheme-[4Fe4S] and deprived of the sulfite; (B) with one-electron reduced siroheme-[4Fe4S] and deprived of the sulfite; (C) with oxidized siroheme-[4Fe4S] and the sulfite ion bound; (D) with one-electron reduced siroheme-[4Fe4S] and the sulfite ion bound.

strictly conserved in the dSIR sequences derived from *Archaeoglobus fulgidus*, *Desulfovibrio gigas*, *Desulfovibrio vulgaris* and *Desulfomicrobium norvegicum*. Multi-sequence alignment for β subunit in turn confirmed the conservation of four cysteines ($C\beta140$, $C\beta177$, $C\beta178$ and $C\beta182$ – Figure 7) coordinating [4Fe4S] cluster. The most extensive crystallographic data are available for dSIR derived from *Archaeoglobus fulgidus*. For *A. fulgidus* are available dSIR crystal structures with substrate: sulfite, final product: sulfide, as well as with molecules, i.e. CN^-, CO, NO_2^-, NO_3^-, which may simulate intermediates of sulfite reduction and their interactions with active site residues). The multi-sequence alignments revealed that the most important

residues within dSIR active site are strictly conserved in sequences of all crystal structures available in the PDB database, thus we chose crystal structure of dSIR in complex with sulfite anion (PDB code: 3MM5, resolution of 1.80 Å)[25] derived from *Archaeoglobus fulgidus* for QM study focused on the mechanism of sulfite reduction.

Siroheme-[4Fe4S] Cofactor and Substrate Binding

Theoretical studies began with optimizing the enzyme-substrate (ES) complex using models of various sizes and establishing a size sufficient to model the reaction catalyzed in the active site of the dSIR representatives. The ES complex was optimized for medium (Figure 7C, D) and large (Supplementary Data) models with two versions of siroheme-[4Fe4S] cofactor (Figure 6): oxidized (formally Fe(III)-siroheme-[4Fe4S]) and one-electron reduced (formally Fe(II)-siroheme-[4Fe4S]). For the small and medium models siroheme-[4Fe4S] cofactor was optimized in the absence of substrate in order to investigate how the binding of sulfite substrate affects the siroheme-[4Fe4S] spin distribution. For the small model the oxidized and reduced siroheme-[4Fe4S] cofactor was optimized with and without the constraints imposed on the hydrogen atoms replacing propionates from siroheme and the Cα of [4Fe4S] ligands to check whether the geometry of the siroheme-[4Fe4S] cofactor determined by the dSIR active site affects its electronic configuration. The results obtained for the small model showed that regardless of whether the positions of the siroheme and cysteine ligands were constrained or not, similar spin distributions were obtained for the oxidized and reduced siroheme-[4Fe4S]-cofactor.

Oxidized siroheme-[4Fe4S] cofactor was characterized as containing siroheme high spin iron in oxidation state between Fe(II) and Fe(III) (Fe(SRM) in Figure 6 and Figure 7A, C), and [4Fe4S] containing two high spin Fe(III) (Fe1 and Fe4 in Figure 6 and Figure 7A, C), one high spin Fe(II) (Fe3 in Figure 6 and Figure 7A, C) and one iron ion in state between Fe(II) and Fe(III) (Fe2 in Figure 6 and Figure 7A, C). The spin distribution for oxidized cofactor observed in the small model was preserved in the medium model deprived of HSO_3^- anion, as well as in the medium model and large model including HSO_3^- (Figure 6). This result indicates that the oxidized state is a stable state of siroheme-[4Fe4S] cofactor, which is supported by the EPR spectroscopy results.[38,39] The QM calculations revealed additionally that spin distribution within the oxidized siroheme-[4Fe4S] cofactor is preserved regardless of the size of the considered model (insensitive to the interactions with protein surroundings) or even substrate binding.

One-electron reduction of oxidized siroheme-[4Fe4S] cofactor provides more varied results for electronic configuration in the models considered. In the small model, spin population is almost evenly distributed among all the iron cations in reduced siroheme-[4Fe4S] cofactor taking values from 3.69 (Fe2) to 3.77 (Fe(SRM) in Figure 6). Interestingly, optimization of medium model without HSO_3^- results in a structure containing oxidized siroheme-[4Fe4S] cofactor and a radical formed on Rα170 (Figure 6 and Figure 7B) suggesting that an electron delivered to the active site cannot reduce the siroheme-[4Fe4S] cofactor until the substrate is bound. The optimization of medium model with HSO_3^- bound (Figure 7D) revealed reduced siroheme-[4Fe4S] cofactor containing the lowest spin population on Fe3 (3.67) and the highest on Fe4 (3.78). Such tendency in spin distribution within reduced siroheme-[4Fe4S] cofactor is maintained in the large model (Figure 6), i.e. the lowest spin population on Fe3 (3.66) and the highest on Fe4 (3.84).

Summarizing, the obtained results revealed that one-electron reduction of siroheme-[4Fe4S] cofactor is only possible after substrate binding and what is more important the delivery of an electron does not affect the spin population on siroheme iron, which is maintained in Fe(II)/(III) state (spin population of 3.72–3.75 in oxidized and reduced versions of cofactor), but influences the spin populations within the [4Fe4S] cluster (Figure 6). Moreover, preliminary studies have shown that the medium model seems to be sufficient to model the reduction reaction, as it qualitatively reproduces the distribution of the spin population in the oxidized and reduced siroheme-[4Fe4S] cofactor observed in the large model.

The Concept of the Sulfite Reduction Mechanism

Based on the crystallographic studies it has been suggested that the electrons necessary for the reduction of sulfite to sulfide are provided by oxidation of two conserved cysteines from the C-terminus of the DsrC protein, which is also considered as a γ subunit of dSIR (Figure 2).[22] The DsrC protein in turn acquires electrons and protons through interaction with DsrMKJOP membrane complex with disulfide/thiol reductase activity.[53] The crystallographic studies revealed that DsrC binds to the $(\alpha\beta)_2$ heterotetramer of dSIR, positioning C-terminal conserved cysteine in the vicinity of functional siroheme ring. This fact was taken into account in the present consideration of dSIR mechanism by checking the energy needed to oxidize two cysteines, leading to the formation of a disulfide bond and release of two hydrogen atoms. In order to calculate the energy of two-electron oxidation of the two conserved cysteines present at the C-terminus of the DsrC protein, a small QM model containing only these two cysteines was constructed. Computations were performed using the same level of theory as applied to the models of dSIR active site. The results revealed that the release of the first hydrogen atom costs 82.1 kcal/mol, while the binding energy of the second hydrogen atom is only 27.5 kcal/mol (thus releasing two hydrogen atoms requires 109.6 kcal/mol). This result indicates that the release of a proton and an electron initiates the transfer of the remaining proton and electron and leads to the formation of a disulfide bond. This is consistent with the observation from the previous section that the supply of one electron to the active site of dSIR leads to a change in the oxidation state of the [4Fe4S] cofactor, while the sulfur atom from the reactant can only be reduced by delivery of two electrons. In conclusion, it seems reasonable to investigate the dSIR mechanism as three steps of two-electron reduction of sulfite to sulfide, as it reflects the stability of sulfur

compounds at even oxidation states of S. This approach significantly reduces the number of possible intermediates that need to be tested; in subsequent studies it can be further expanded by considering elementary one-electron reduction steps.

Three Steps of Two-Electron Reduction

The starting point for the modeling of the dSIR catalytic reaction is the geometry optimized for the medium model for the ES complex labeled as *R* and presented in Figure 7C. It contains HSO_3^- anion, oxidized siroheme-[4Fe4S] cofactor, positively charged Rα98, Rα170, Kα211 and neutral Kα213, since according to the results of pKa predictions Kα213 (pKa = 6.59) prefers its deprotonated state. In the available crystal structures, Kα211 and Kα213 interact with each other, thus the ES complex was also optimized in a version containing neutral Kα211 and positively charged Kα213, but during geometry optimization proton transfer occurred from Kα213 to Kα211 leading back to *R* structure. The proton located on the HSO_3^- ion is directed towards a 15 Å long water channel that connects the active site with the protein surface (Figure 7C, D).

The QM calculations revealed that proton transfer within *R* structure from Kα211 or Rα170 to HSO_3^- ion, leading to H_2SO_3 is unlikely, because H_2SO_3 is unstable and proton returns to the donor. It was possible to optimize the SO_2-Fe(III)-siroheme-[4Fe4S] intermediate formed as a result of proton transfer from Rα98 to HSO_3^- coupled with the release of a water molecule, but it is by 27.4 kcal/mol less stable than *R*, therefore its formation was excluded from the consideration of feasible mechanism. However, the SO_2-Fe(III)-siroheme-[4Fe4S] intermediate was tested en route to SOOH-Fe(IV)-siroheme-[4Fe4S] or $SOOH^-$-Fe(V)-siroheme-[4Fe4S] intermediates formed by proton transfer from Kα211 or Rα170, but in all tested versions they were unstable (geometry optimizations led back to the the SO_2-Fe(III)-siroheme-[4Fe4S] intermediate), which indicates that sulfur reduction requires delivery of electrons from external source, i.e. electrons available within the Fe(III)-siroheme-[4Fe4S] cofactor are not sufficient.

In the rest of the manuscript, for the sake of readability, the names of the intermediates will appear according to the following key: superscript $^{+XH}$ indicates *X* additional protons, while $^{Y'}$ indicates *Y* additional electrons introduced into the system with respect to *R*.

Delivery of the First Packet of Two Electrons and Two Protons

Delivery of two electrons and two protons to the *R* structure with oxidized siroheme-[4Fe4S] binding HSO_3^- (S(IV)), leads directly to formation of $SOOH^-$-Fe(III)-siroheme-[4Fe4S] with $^-$O-S-OH containing S(II) and release of a water molecule. The QM results indicate that the most stable $SOOH^-$-Fe(III)-siroheme-[4Fe4S] structure ($^{+2H}I1^{2'}$ in Figure 8) contains, similarly to *R*, positively charged Rα98, Rα170, Kα211 and neutral Kα213. We tested also structures with protonated Kα213 and deprotonated either Rα98, Rα170 or Kα211, but all of them turned out to be less stable than $^{+2H}I1^{2'}$ by 13.3, 6.9 and 1.2 kcal/mol, respectively. This result shows that Kα213 and Kα211 can exchange proton during reaction and are the most likely mediators for the transport of protons to HSO_3^-. In all tested scenarios, the two electrons are transported directly to the sulfur atom, leading to its reduction from S(IV) in HSO_3^- ion (*R*) to S(II) in $SOOH^-$ ($^{+2H}I1^{2'}$), while two protons are delivered to the oxygen atom of sulfite, causing dissociation of the water molecule. Coupled delivery of two electron and two protons does not change the oxidation state of the [4Fe4S] cluster, whose spin distribution resembles that for the oxidized state of ES complex (*R* in Figure 7C).

The $^{+2H}I1^{2'}$ containing $SOOH^-$ can be further converted to a complex containing the $S(OH)_2$ intermediate (HO-S-OH) by proton transfer either from Kα211, Rα98 or Rα170. The results revealed that the most likely scenario is a proton transfer from Kα211 leading to $^{+2H}I2^{2'}$ (Figure 8) containing deprotonated Kα211 and Kα213, which is only 1.4 kcal/mol less stable than $^{+2H}I1^{2'}$. This proton transfer occurs with a negligible barrier, and thus in the case of electron deficiency $^{+2H}I2^{2'}$ is a feasible intermediate in the mechanism of trithionate ($S_3O_6^{2-}$) formation (Figure 3). The other scenarios of the formation of $S(OH)_2$ were also tested but the modeled intermediates were unstable (proton returns to the donor) or characterized by significantly higher energy (by 9.9–20.6 kcal/mol than $^{+2H}I1^{2'}$, details in Supplementary Data). All scenarios of further reduction of sulfur S(II) from $SOOH^-$ or $S(OH)_2$ to sulfur S(I) in SOH or sulfur S(0) in SOH^- have been tested and excluded due to the instability of the SOH-Fe(IV)-siroheme-[4Fe4S] and SOH^--Fe(V)-siroheme-[4Fe4S] complexes.

Delivery of the Second Packet of Two Electrons and Two Protons

Subsequent delivery of a set of two electrons and two protons to $^{+2H}I1^{2'}$ containing $SOOH^-$ ($^-$O-S(II)-OH) leads directly to a two-electron reduction of sulfur, release of a water molecule and formation of the SOH^- intermediate (S(0)-OH^-) labeled as $^{+4H}I1^{4'}$ in Figure 8. The results of QM calculations show that among all optimized SOH^--Fe(III)-siroheme-[4Fe4S] structures, the most stable ($^{+4H}I1^{4'}$) contains positively charged Rα98, Rα170, Kα213 and neutral Kα211. The other complexes containing SOH^- intermediates are by 7.2–10.4 kcal/mol less stable than $^{+4H}I1^{4'}$ (details in Supplementary data). Interestingly, SOH^--Fe(III)-siroheme-[4Fe4S] structure containing deprotonated Kα213 is by 8.8 kcal/mol less stable than $^{+4H}I1^{4'}$, which indicates that Kα211 may be involved in the delivery of proton to $SOOH^-$ and/or dissociation of water molecule. As in the previous reaction step, transfer of two electrons and two protons to the $^{+2H}I1^{2'}$ complex does not affect the spin populations observed on siroheme-[4Fe4S] cofactor, which remains oxidized like *R* in Figure 7C.

As with the previous oxidation states of the active site, evolution of the $^{+4H}I1^{4'}$ by providing a proton to SOH^- from adjacent positively charged residues (Rα98, Rα170, Kα213) was

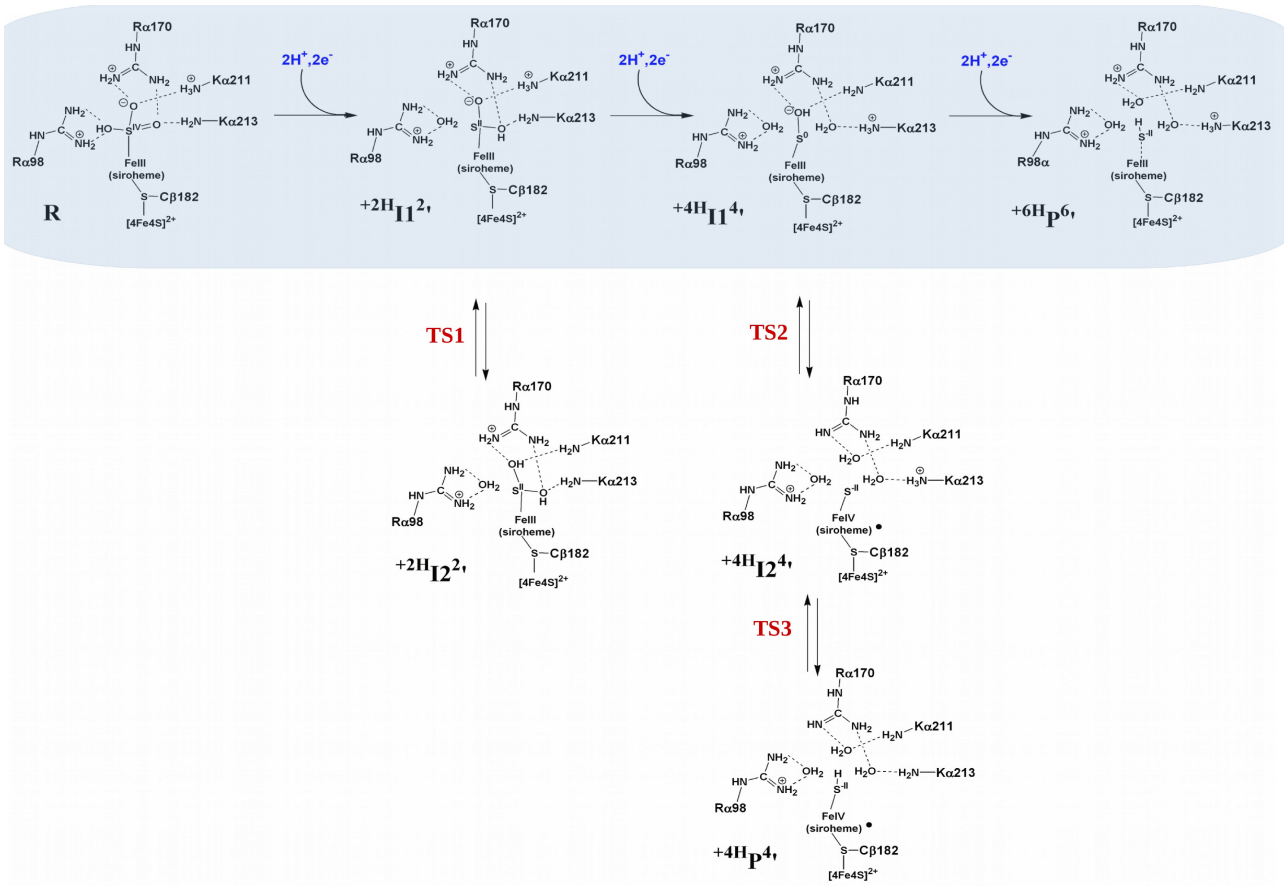

Figure 8. Scheme of the dSIR catalytic reaction considered as three steps of two-electron reduction, obtained on the basis of the performed QM calculations.

also tested. The QM calculations reveal that proton transfer from Rα170 to S(O)-OH^- in $^{+4H}I1^{4'}$ leads to the formation of S(-II) bound to the siroheme-[4Fe4S] cofactor ($^{+4H}I2^{4'}$ in Figure 8) and the release of water molecule. The $^{+4H}I2^{4'}$ contains positively charged Rα98, Kα213 and deprotonated (neutral) Kα211 and Rα170. Spin populations observed for $^{+4H}I2^{4'}$ (see Supplementary data) indicate that it can be written as S^{-2}-Fe(IV)-siroheme radical-[4Fe4S], thus the two electrons used for sulfur reduction come from siroheme iron and siroheme ring. Interestingly, in the $^{+4H}I2^{4'}$ structure the [4Fe4S] cluster maintains the distribution of spin populations observed in all intermediates described so far and reported for *R* in Figure 7C. The S^{-2}-Fe(IV)-siroheme radical-[4Fe4S] is only by 0.5 kcal/mol more stable than $^{+4H}I1^{4'}$, but its formation is associated with a relatively high energy barrier of 15.1 kcal/mol due to the dissociation of an S–O bond and the associated change of oxidation state of sulfur. Protonation of S^{2-} by Kα213 leads from $^{+4H}I2^{4'}$ to the $^{+4H}P^{4'}$ structure containing sulfide anion (SH^-) bound to the Fe(IV)-siroheme radical-[4Fe4S], deprotonated Rα170, Kα211, Kα213 and positively charged Rα98. The formation of $^{+4H}P^{4'}$, which is by 5.9 kcal/mol less stable than $^{+4H}I2^{4'}$, is connected with a barrier of 7.0 kcal/mol (TS3 in Figure 8). The remaining scenarios for the formation of S^{-2}-Fe(IV)-siroheme radical-[4Fe4S] and SH^--Fe(IV)-siroheme radical-[4Fe4S] were energetically less favorable, so they were omitted from this description (Supplementary Data).

Delivery of the Third Packet of Two Electrons and Two Protons

The final step of sulfite to sulfide reduction is delivery of the third set of two electrons and two protons to the $^{+4H}I1^{4'}$ complex containing neutral Kα211 and S(0)-OH^-, which leads to the two-electron reduction of sulfur atom, release of a water molecule and production of the sulfide anion (HS^-). The most stable enzyme-product (EP) complex, labeled as $^{+6H}P^{6'}$ (Figure 8) contains, similarly to $^{+4H}I1^{4'}$, neutral Kα211 and positively charged Rα98, Rα170 and Kα213. The other versions of EP complex containing neutral Kα213 or Rα98 are characterized by very similar final energies, which are by 0.1 and 1.8 kcal/mol higher than $^{+6H}P^{6'}$, respectively. The least likely intermediary in proton transfer to SOH^- is Rα170, because the EP structure containing deprotonated Rα170 is by 7.0 kcal/mol less stable than $^{+6H}P^{6'}$. Similarly to the previous reaction step, transfer of two electrons and two protons to the $^{+4H}I1^{4'}$ complex does not affect the spin populations on siroheme-[4Fe4S] cofactor, which maintains the oxidation state observed in the ES (Figure 7C).

Summary of the Considered dSIR Mechanism

Summarizing, the performed QM studies showed that the reduced form of siroheme-[4Fe4S] can only be obtained if one electron is supplied from an external source to the ES complex. Moreover, the electronic configurations of R0′ (Figure 7B) and R′ (Figure 7D) indicate that the presence of sulfite bound to the siroheme is necessary for the one-electron reduction of the siroheme-[4Fe4S] cofactor. This observation is consistent with the conclusion drawn from EPR experiments that oxidized siroheme-[4Fe4S] is the resting state of dSIR active site.[38,39] The present study revealed that progress of the catalytic reaction associated with sulfur reduction is only possible when two electrons are available, thus we suspect that reduced siroheme-[4Fe4S] cofactor can be observed only during *in vitro* experiments in conditions of deficiency of electrons. Under electron-deficiency conditions the reaction stops at the stage of the ES complex, which in turn made it possible to obtain its crystal structures, which are available in the Protein Data Bank. The results of QM studies carried out for the mechanism of coupled transfer of two electrons and two protons in three sets support the hypothesis formulated based on crystallographic studies that the siroheme-[4Fe4S] site does not undergo major geometric rearrangements[1,25] and presumably retains its electronic configuration throughout the main intermediates defining the reaction mechanism.

dSIR Catalytic Cycle

The energy diagram presented in Figure 9 was constructed according to the method proposed by Per Siegbahn and Margareta Blomberg[54] and includes the final energies of the most stable stationary points of dSIR cycle corrected for the energetic costs of substrates binding (HSO_3^-, $6H^+$, $6e^-$) and releasing of products ($3H_2O$, HS^-). Therefore, the following data were used to estimate the final energies presented in Figure 9 of the states of active sites involved in the dSIR catalytic cycle: i) final zero-point corrected electronic energies of the presented stationary points optimized using the medium model; ii) electronic energies (computed with the same method as final energies of the stationary points) of the following species: hydrogen atom, water molecule, sulfite (HSO_3^-) and sulfide (HS^-) anions; iii) the hydration energy computed using SMD model[55] for water molecule, sulfite (HSO_3^-) and sulfide (HS^-) anions; iv) the energy required for two-electron oxidation of

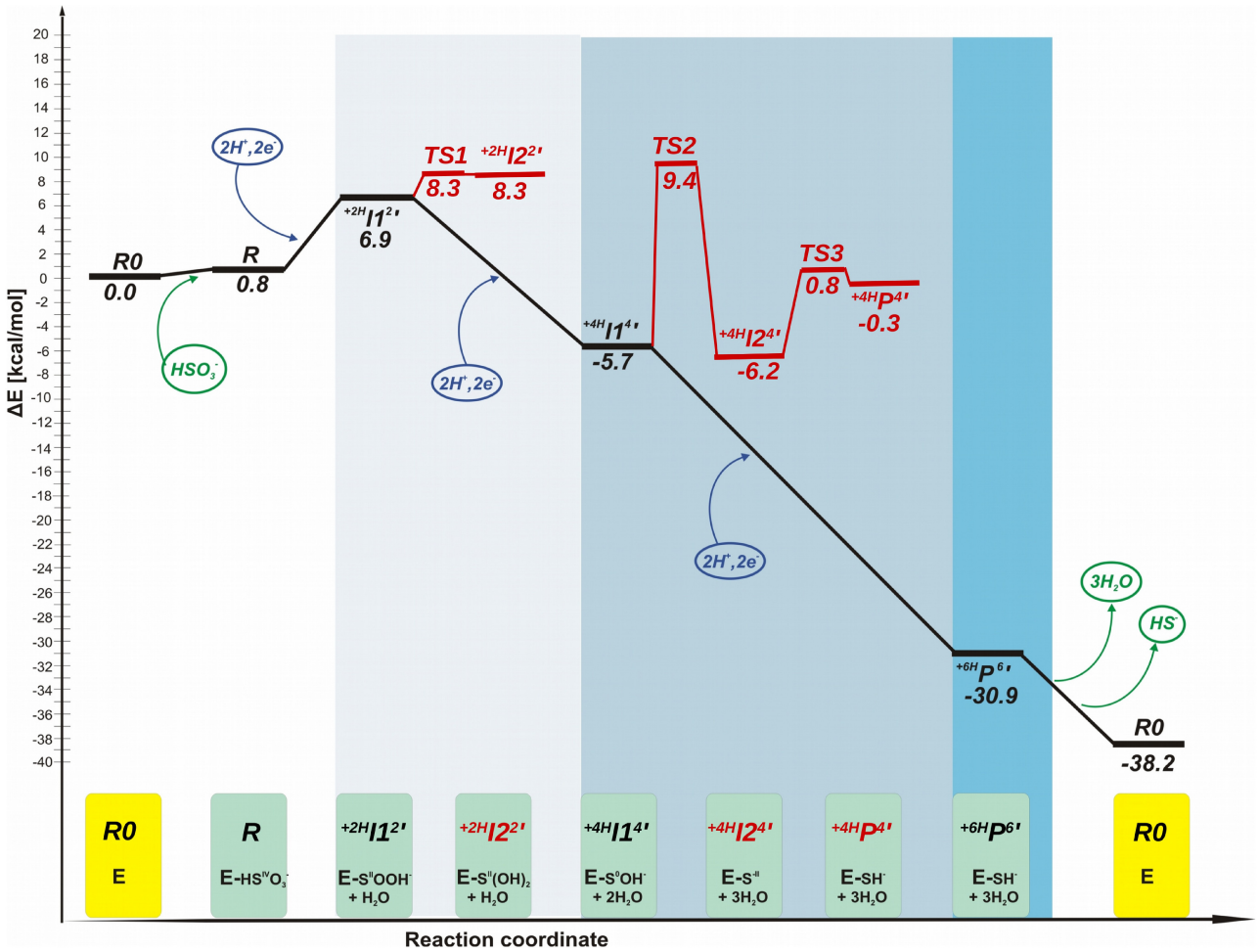

Figure 9. Energy diagram presenting dSIR catalytic cycle considered according to the mechanism, where three sets of two electrons and two protons are delivered to the dSIR active site.

two cysteines from DsrC protein (provides the electrons end protons required for catalytic reaction of dSIR), formation of disulfide bond and dissociation of two hydrogen atoms. It was computed that energy required for this process to occur equals 109.6 kcal/mol (82.1 kcal/mol for the first hydrogen atom and 27.5 kcal/mol for second H atom).

The energy diagram revealed that reduction of sulfite to sulfide produces an energy of 38.2 kcal/mol, which is reasonably consistent with the experimental standard Gibbs free energy change for the reduction of sulfite to sulfide ($\Delta G'^0 = -36.4$ kcal/mol[15]) and gives an error of 1.8 kcal/mol. The rate limiting step of the thus far recognized reaction mechanism is formation of the $^{+2H}I1^{2'}$ ($SOOH^-$-Fe(III)-siroheme-[4Fe4S]) intermediate as a result of the delivery of the first set of two electrons and two protons from the DsrC protein. Therefore, this reaction step was tested in more detail and decomposed into two steps of coupled electron and proton transfer. For this purpose, we optimized various variants of intermediates resulting from the acceptance of one electron and one proton by the ES complex (*R*). Among all optimized structures, the most stable is intermediate labeled as $^{+H}I1'$ and containing neutral Kα213, SO_2 bound to the Fe(II) of siroheme and the [4Fe4S] cluster with the distribution of spin populations observed in *R* (Supplementary Data). For comparison, structure $^{+H}R'$, obtained from *R* by protonation of Kα213 and reduction of siroheme-[4Fe4S] cofactor is by 8.6 kcal/mol less stable than $^{+H}I1'$. However, taking into account the energy of the release of the first electron and proton from the DsrC protein (82.1 kcal/mol) makes $^{+H}I1'$ 39.6 kcal/mol less stable than *R*, which argues against this intermediate. Interestingly, the observation of the enzyme *in vitro* shows that dSIR extracted from the soluble fraction catalyzes formation of the mixture of sulfide (SH^-), $S_3O_6^{2-}$ and $S_2O_3^{2-}$,[29] which may indicate the existence of an internal electron source in the dSIR enzyme, independent of the presence of membrane proteins. The internal electron source can also support the reaction path leading from $^{+4H}I1^{4'}$ to $^{+H}P^{4'}$ (Figures 8 and 9) by making up for the electron deficiency appearing on the siroheme ring in $^{+4H}I2^{4'}$ intermediate (Figure 8). The presence of the additional [4Fe4S] cluster within ferredoxin domain[22] in close vicinity of the siroheme-[4Fe4S] site (13.5 Å, Figure 5) makes such support of the catalysis by supplying an electron from an internal source possible. Unfortunately, the redox potential of [4Fe4S] cluster from A3/B3 ferredoxin like domains is unknown, thus, we are not able to include it in computational results as an alternative source of electrons for the dSIR reaction. Considering the generally low redox potentials for [4Fe4S] in ferredoxins,[56] we suspect that a single electron is easier to obtain from ferredoxin [4Fe4S] than from the DsrC protein, while protons are accessible through four protonable residues (Rα98, Rα170, Kα211, Kα213). The present QM results revealed that during dSIR catalysis sulfur can be only reduced through two-electron steps, thus delivery of one electron is connected with reduction of siroheme-[4Fe4S] cofactor, which in turn, according to the EPR experiments, is less stable in its reduced form.[38,39] Therefore, the acceptance of a single electron by an active site containing a reduced siroheme-[4Fe4S] cofactor with bound sulfur intermediate appears to be more energetically favorable than the delivery of a single electron to the same complex with oxidized siroheme-[4Fe4S] cofactor. Following this line of reasoning, it seems tempting to hypothesize that the [4Fe4S] cluster from the B3 ferredoxin domain supports or initiates the supply of electrons from the DsrC protein.

Conclusions

Summarizing, the results obtained from QM calculations in combination with the available literature data lead to several interesting conclusions regarding the course of the reaction of sulfite to sulfide reduction catalyzed by dSIR. The QM calculations were performed to test the mechanism of dSIR reaction assuming the delivery of six electrons and six protons in three packets of two electrons and two protons. Importantly, the QM results showed that the two-electron packets delivered to the active site go directly to the reactant, which means that the electronic configuration of the siroheme-[4Fe4S] cofactor does not change for the main reaction intermediates formed during the catalytic cycle. Moreover, the results revealed that among four protonable residues interacting with HSO_3^- ion, Kα213 and Kα211 are the best mediators in transport of protons required for sulfite reduction. The computed energy of catalytic reaction (−38.2 kcal/mol) is in a good agreement with experimental standard Gibbs free energy change for the reduction of sulfite to sulfide (−36.4 kcal/mol).[15] Each major reaction step is initiated by delivery of two protons and two electrons, and leads from $HS^{IV}O_3^-$ (*R*) through $S^{II}OOH^-$ ($^{+2H}I1^{2'}$) and S^0OH^- ($^{+4H}I1^{4'}$) to $S^{-II}H^-$ ($^{+6H}P^{6'}$). After delivering each two-electron and two-proton package, possible evolutions of the system were considered and the most energetically favorable paths are presented in Figures 8 and 9. The remaining intermediates are gathered in the Supplementary Data. The results revealed that in all stable intermediates sulfur occurs only in the following oxidation states: IV, II, 0, -II. Considering the mechanism leading from $^{+4H}I1^{4'}$ to $^{+H}P^{4'}$ (modeled as occurring after delivery of the second packet of two-electron and two-proton), it is energetically more favorable for the system to take second electron from the siroheme ring, causing the formation of a siroheme radical, than to allow one-electron reduction of sulfur ($^{+4H}I2^{4'}$ and $^{+4H}P^{4'}$ in Figure 8), which supports hypothesis of reduction of sulfur in two-electron steps. However, it should be borne in mind that although sulfur in the considered system tends to undergo two-electron reduction, the active site can be reduced sequentially in one-electron steps. In this case, the electron will be stored within the siroheme-[4Fe4S] cofactor, which was also tested in the present study for the ES complex. In the ES-complexes resulting from the delivery of one electron and one proton, the [4Fe4S] cluster from siroheme-[4Fe4S] is reduced, while the spin populations on siroheme remains maintained in the range of 3.71–3.73 in both oxidized and one-electron reduced siroheme-[4Fe4S] cofactors. Interestingly, in $^{+H}I1'$ containing $S^{IV}O_2$ bound (formed from $^{+H}R'$ by proton transfer from Kα213 and dissociation of water molecule), the stored electron is transferred within siroheme-[4Fe4S] cofactor from

the [4Fe4S] cluster to siroheme iron decreasing its spin population from 3.71 in $^{+H}$R′ to 3.43 in $^{+H}$I1′ (Supplementary Data). In this case, the supply of another electron through the ferredoxin domain would enable a two-electron reduction of $S^{IV}O_2$.

The presented theoretical study show that the mechanism of sulfite to sulfide reduction catalyzed in the dSIR active site feasibly occurs in three steps of two-electron sulfur reduction. However, this does not involve the need to deliver two-electron and two-proton packets to the active site because the cofactor can store an electron until another electron is delivered to the system to ensure two-electron reduction of the reaction intermediate. Therefore, to obtain a full picture of the reaction catalyzed by dSIR, the here proposed major two-electron/two-proton steps with their stable reaction intermediates should be supplemented in future with a description of chemical transformations/electronic structure changes elicited by single electron/single proton transfer steps.

Abbreviations

QM	quantum-mechanical
DFT	Density Functional Theory
PCM	polarisable continuum model
ZPE	zero-point energy
APSR	adenosine 5′-phosphosulfate reductase
APS	adenosine 5′-phosphosulfate
AMP	adenosine 5′-monophosphate
ATP	adenosine 5′-triphosphate
dSIR	dissimilatory sulfite reductase
ES	enzyme-substrate complex
EP	enzyme-product complex
SRM	siroheme
PDB	Protein Data Bank

Acknowledgements

The Swedish Nuclear Fuel and Waste Management Co (SKB) is acknowledged for financial support. This research was supported in part by PLGrid Infrastructure.

Conflict of Interests

The authors declare that they have no conflicts of interest with the contents of this article.

Data Availability Statement

Cumulative results for all tested potential intermediates whose description was omitted from the main text of the manuscript; Energies and Cartesian coordinates for the most important stationary points of considered dSIR models. The data that support the findings of this study are available in the supplementary material of this article.

Keywords: density functional calculations · reductase · siroheme · sulfate respiration · sulfite reduction

[1] K. Parey, G. Fritz, U. Ermler, P. M. H. Kroneck, *Metallomics* **2013**, *5*, 302.
[2] L. Prioretti, M. Giordano, *J. Phycol.* **2016**, *52*, 1094.
[3] Y. L. Chiang, Y. C. Hsieh, J. Y. Fang, E. H. Liu, Y. C. Huang, P. Chuankhayan, J. Jeyakanthan, M. Y. Liu, S. I. Chan, C. J. Chen, *J. Bacteriol.* **2009**, *191*, 7597.
[4] G. Gibson, J. Cummings, G. Macfarlane, *FEMS Microbiol. Ecol.* **1991**, *86*, 103.
[5] W. A. Hamilton, *Biodegradation* **1998**, *9*, 201.
[6] F. Kuang, J. Wang, L. Yan, D. Zhang, *Electrochim. Acta* **2007**, *52*, 6084.
[7] Y. Taguchi, M. Sugishima, K. Fukuyama, *Biochemistry* **2004**, *43*, 4111.
[8] H. Takahashi, S. Kopriva, M. Giordano, K. Saito, R. Hell, *Annu. Rev. Plant Biol.* **2011**, *62*, 157.
[9] M. Giordano, J. A. Raven, *Aquat. Bot.* **2014**, *118*, 45.
[10] L. Prioretti, B. Gontero, R. Hell, M. Giordano, *Front. Plant Sci.* **2014**, *5*, 597.
[11] J. R. Postgate, *The Sulfate-Reducing Bacteria (2nd Edition)*, Cambridge University Press, Cambridge **1984**.
[12] W. Dou, R. Jia, P. Jin, J. Liu, S. Chen, T. Gu, *Corros. Sci.* **2018**, *144*, 237.
[13] W. Dou, Y. Pu, X. Han, Y. Song, S. Chen, T. Gu, *Bioelectrochemistry* **2020**, *133*, 107478.
[14] A. Wójcik-Augustyn, A. J. Johansson, T. Borowski, *Comput. Struct. Biotechnol. J.* **2019**, *17*, 770.
[15] R. K. Thauer, K. Jungermann, K. Decker, *Bacteriol. Rev.* **1977**, *41*, 100.
[16] C. Dahl, H. G. Koch, O. Keuken, H. Trüper, *FEMS Microbiol. Lett.* **1990**, *67*, 27.
[17] A. Schiffer, G. Fritz, P. M. H. Kroneck, U. Ermler, *Biochemistry* **2006**, *45*, 2960.
[18] A. Wójcik-Augustyn, A. J. Johansson, T. Borowski, *Biochimica et Biophysica Acta (BBA) – Bioenergetics* **2021**, *1862*, 148333.
[19] J. LeGall, G. Fauque, ed. A. J. B. Zehnder, Wiley, New York, *Biology of Anaerobic Microorganisms* **1988**, pages 587–639.
[20] J. Steuber, A. F. Arendsen, W. R. Hagen, P. M. Kroneck, *Eur. J. Biochem.* **1995**, *233*, 873.
[21] J. Steuber, A. F. Arendsen, W. R. Hagen, P. M. Kroneck, *Structure* **2003**, *11*, 1133.
[22] T. F. Oliveira, C. Vonrhein, P. M. Matias, S. S. Venceslau, I. A. C. Pereira, M. Archer, *J. Biol. Chem.* **2008**, *283*, 34141.
[23] G. J. Mander, M. S. Weiss, R. Hedderich, J. Kahnt, U. Ermler, E. Warkentin, *FEBS Lett.* **2005**, *579*, 4600.
[24] J. R. Cort, S. V. Mariappan, C. Y. Kim, M. S. Park, T. S. Peat, G. S. Waldo, T. C. Terwilliger, M. A. Kennedy, *Eur. J. Biochem.* **2001**, *268*, 5842.
[25] K. Parey, E. Warkentin, P. M. H. Kroneck, U. Ermler, *Biochemistry* **2010**, *49*, 8912.
[26] B. R. Crane, L. M. Siegel, E. D. Getzoff, *Biochemistry* **1997**, *36*, 12120.
[27] C. Dahl, N. M. Kredich, R. Deutzmann, H. G. Trlfper, *J. Gen. Microbiol.* **1993**, *139*, 1817.
[28] H. L. Drake, J. M. Akagi, *J. Bacteriol.* **1978**, *133*, 916.
[29] J. Steuber, H. Cypionka, P. M. H. Kroneck, *Arch. Microbiol.* **1994**, *162*, 255.
[30] J. Ostrowski, J. Y. Wu, D. C. Rueger, B. E. Miller, L. M. Siegel, N. M. Kredich, *J. Biol. Chem.* **1989**, *264*, 15726.
[31] B. R. Crane, E. D. Getzoff, *Opin. Struct. Biol.* **1996**, *6*, 744.
[32] P. A. Janick, L. M. Siegel, *Biochemistry* **1982**, *21*, 3538.
[33] I. Moura, J. LeGall, A. R. Lino, H. D. Peck, G. Fauque, A. V. Xavier, D. V. DerVartanian, J. J. G. Moura, B. H. Huynh, *J. Am. Chem. Soc.* **1988**, *110*, 1075.
[34] R. Silaghi-Dumitrescu, S. V. Makarov, *Int. J. Quantum Chem.* **2012**, *112*, 900.
[35] B. R. Crane, L. M. Siegel, E. D. Getzoff, *Science* **1995**, *270*, 59.
[36] B. R. Crane, L. M. Siegel, E. D. Getzoff, *Biochemistry* **1997**, *36*, 12101.
[37] B. R. Crane, H. Bellamy, E. D. Getzoff, *Acta Crystallogr.* **1997**, *53*, 8.
[38] A. M. V. Brânzanic, U. Ryde, R. Silaghi-Dumitrescu, *J. Inorg. Biochem.* **2020**, *203*, 110928.
[39] L. M. Siegel, D. C. Rueger, M. J. Barber, R. J. Krueger, N. R. Orme-Johnson, W. H. Orme-Johnson, *J. Biol. Chem.* **1982**, *257*, 6343.
[40] J. A. Christner, E. Münck, P. A. Janick, L. M. Siegel, *J. Biol. Chem.* **1981**, *256*, 2098.

[41] S. N. Khan, A. Griffith, F. De Proft, E. Miliordos, R. W. A. Havenith, D. Bykov, A. V. Cunha, *Phys. Chem. Chem. Phys.* **2022**, *24*, 18543.
[42] M. R. A. Blomberg, T. Borowski, F. Himo, R.-Z. Liao, P. E. M. Siegbahn, *Chem. Rev.* **2014**, *114*, 3601.
[43] W.-J. Wei, R.-Z. Liao, *ChemCatChem* **2024**, page e202301712.
[44] X. Sheng, F. Himo, *Acc. Chem. Res.* **2023**, *56*, 938.
[45] P. E. M. Siegbahn, *FEBS Lett.* **2023**, *597*, 38.
[46] C. R. Sondergaard, M. H. Olsson, M. Rostkowski, J. H. Jensen, *J. Chem. Theory Comput.* **2011**, *7*, 2284.
[47] M. H. M. Olsson, C. R. Sondergaard, M. Rostkowski, J. H. Jensen, *J. Chem. Theory Comput.* **2011**, *7*, 525.
[48] M. J. Frisch, G. W. Trucks, H. B. Schlegel, G. E. Scuseria, M. A. Robb, J. R. Cheeseman, G. Scalmani, V. Barone, G. A. Petersson, H. Nakatsuji, X. Li, M. Caricato, A. V. Marenich, J. Bloino, B. G. Janesko, R. Gomperts, B. Mennucci, H. P. Hratchian, J. V. Ortiz, A. F. Izmaylov, J. L. Sonnenberg, D. Williams-Young, F. Ding, F. Lipparini, F. Egidi, J. Goings, B. Peng, A. Petrone, T. Henderson, D. Ranasinghe, V. G. Zakrzewski, J. Gao, N. Rega, G. Zheng, W. Liang, M. Hada, M. Ehara, K. Toyota, R. Fukuda, J. Hasegawa, M. Ishida, T. Nakajima, Y. Honda, O. Kitao, H. Nakai, T. Vreven, K. Throssell, J. A. Montgomery Jr., J. E. Peralta, F. Ogliaro, M. J. Bearpark, J. J. Heyd, E. N. Brothers, K. N. Kudin, V. N. Staroverov, T. A. Keith, R. Kobayashi, J. Normand, K. Raghavachari, A. P. Rendell, J. C. Burant, S. S. Iyengar, J. Tomasi, M. Cossi, J. M. Millam, M. Klene, C. Adamo, R. Cammi, J. W. Ochterski, R. L. Martin, K. Morokuma, O. Farkas, J. B. Foresman, D. J. Fox, Gaussian 16, Revision A.03, Gaussian Inc., Wallingford CT **2016**.
[49] S. Grimme, J. Antony, S. Ehrlich, H. Krieg, *J. Chem. Phys.* **2010**, *132*, 154104.
[50] S. Grimme, S. Ehrlich, L. Goerigk, *J. Comput. Chem.* **2011**, *32*, 1456.
[51] F. Weigend, R. Ahlrichs, *Phys. Chem.* **2005**, *7*, 3297.
[52] J. Tomasi, B. Mennucci, R. Cammi, *Chem. Rev.* **2005**, *105*, 2999.
[53] R. H. Pires, S. S. Venceslau, F. Morais, M. Teixeira, A. V. Xavier, I. A. C. Pereira, *Biochemistry* **2006**, *45*, 249.
[54] P. E. M. Siegbahn, M. R. A. Blomberg, *Modeling of Mechanisms for Metalloenzymes where Protons and Electrons Enter or Leave; chapter 3 in book: Computational Modeling for Homogeneous and Enzymatic Catalysis*, Wiley-VCH Verlag GmbH & Co. KGaA **2008**.
[55] A. V. Marenich, C. J. Cramer, D. G. Truhlar, *J. Phys. Chem. B* **2009**, *113*, 6378.
[56] H. Beinert, *J. Biol. Inorg. Chem.* **2000**, *5*, 2.

Manuscript received: March 22, 2024
Revised manuscript received: April 10, 2024
Accepted manuscript online: April 11, 2024
Version of record online: May 18, 2024